

Rider control identification in bicycling, parameter estimation of a linear model using lateral force perturbation tests

A.L.Schwab[∞], P.D.L. de Lange[∞], R. Happee^{*}, Jason K. Moore[#]

[∞] Laboratory for Engineering Mechanics
^{*} BioMechanical Engineering
Delft University of Technology
Mekelweg 2, NL 2628 CD Delft, The Netherlands
email: a.l.schwab@tudelft.nl

[#] Sports Biomechanics Lab
Mechanical and Aerospace Engineering
University of California, Davis
One Shields Avenue
Davis, CA 95616-5295, USA

ABSTRACT

Rider control in bicycling is modeled by first adding the rider as a passive mechanism to the Whipple bicycle model. Next, for the rider control model a linear PID controller with or without delay is assumed, where the control inputs are the bicycle lean angle and steer angle with their higher derivatives, and the control output is the action-reaction steer torque applied by the rider at the handle bars. Experimental data is obtained from riding a bicycle on a narrow treadmill while applying an intermitted lateral perturbation by means of an impulse force applied at the seat post. The experiments are conducted in both the stable and the unstable forward speed range. A parametric control model is fitted to the data. The identified parameters, after reduction, stabilize the system and seem to mimic realistic rider control behavior.

1 INTRODUCTION

Balancing a bicycle in motion is an acquired skill which is poorly understood. Multibody dynamic models of the uncontrolled bicycles have provided fundamental insight into bicycle stability in relation to speed and geometry [1, 2]. Further insight into human control is needed, e.g. to design bicycles, possibly with augmented control, minimizing risks of falling. In particular we need to better understand which sensory information is used by the rider, and how this information is used in the combined steering and stabilization task.

The research in human rider control in bicycles and motorcycles started in the seventies during the renewed interest in cybernetics [3, 4, 5, 6]. Among the first were Van Lunteren & Stassen [3] who used a stationary bicycle setup, mimicking normal bicycling, to investigate the influence of drugs and alcohol on the performance of the rider. With the same setup they used system identification techniques to identify the rider control at one fixed forward speed, where they adequately described the rider as a linear PID controller with delay. Rice & Roland [4] measured rider control behavior after an initial lateral perturbation at various speeds on various bicycles and compared the results to computer simulations. Weir [5] used a computer model of a motorcycle rider combination to identify the transfer functions of the various control input-output relations, and concluded that steer torque response to lean angle error is the easiest way to balance a motorcycle in motion. The first to do an actual validation of a rider-vehicle model was Eaton [6], who carried out experiments to validate the theoretical Sharp [7] motorcycle model (including tires) and the rider control crossover model by Weir [5]. After these pioneering studies, most attention has been directed to high-speed motorcycle rider control for reasons of traffic safety [8]. However, the act of balancing at low speed, as is the case for bicycles, has been given little attention. Only this decade, the research on low speed human rider control in bicycling was started again at TU Delft and UC Davis, by observing motions of various rider-bicycle combinations while balancing a bicycle in motion on a large treadmill [9].

Currently there are two main modeling approaches on human rider control in bicycling. One builds on the well-developed quasi-linear aircraft pilot and car driver model as developed by McRuer *et al.* [10, 11, 12] and are transferred to the control of a bicycle. The other is more about intermittent control, where the rider has no action until a certain threshold and then performs an impulsive like action (e.g. Doyle [13]). Such systems are essentially nonlinear, and parallels can be drawn with the recent human postural balance research by Milton [14]. Here we have investigated the validity of the first type of models, that is, a linear controller with or without delay.

The outline of the paper is as follows. After this introduction the model of the bicycle-rider combination which is used in the system identification process is presented. Then the method of the applied system identification techniques are discussed. Next the measurements are briefly discussed after which the results of the system identification are presented. The paper ends with a discussion of the results and some conclusions.

2 METHODS

For the rider model we assume a linear PID controller with or without delay, where the control inputs are the bicycle lean and steer angle with their higher derivatives, and the control output is the steer torque. The rider is assumed to be rigidly attached to the rear frame. The experimental data is obtained from UC Davis [15], where experiments concerning rider control in bicycling are in progress. In the here used experiments, the bicycle is ridden on a narrow treadmill and intermittently laterally perturbed by an impulsive force at the seat post, see Figure 1. First a nonparametric final impulse response (FIR) model is derived, which served as a platform for subsequent parametric modeling. Next the parametric model is fitted to the non parametric model using the steer angle signal. The experiments were done at three forward speeds: 3.2, 4.3 and 7.4 m/s, and by such covering both unstable and stable lateral motions.

3 EXPERIMENTAL SETUP

At UC Davis a measurement bicycle is constructed, which is fully equipped with a number of sensors to measure the state and rider input, see Figure 1. In addition, a perturbator mechanism is present, which is used to excite the system. These perturbations are applied by laterally pulling a rope with a force sensor in series, which is attached on the seat post. The measurement bicycle has the following characteristics: the upper body lean is constrained by rigidly fixing the upper body with a harness to the bicycle frame in order to mimic the rigid rider bicycle model (Whipple model) as best as possible. Next, the knees are fixed to the bicycle frame, which prevents the lateral knee movement which was observed in [16]. And the bicycle is electrically driven, so the rider does not need to exert pedaling power and thus eliminates the need for lower limb movement.

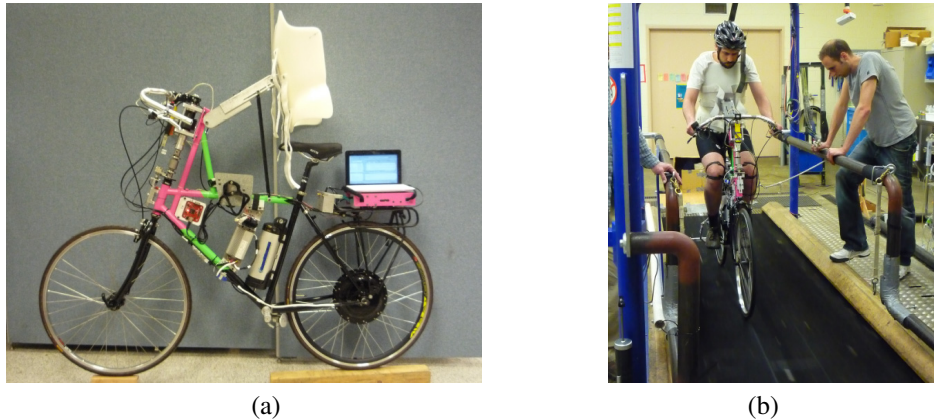


Figure 1. a): Instrumented and actuated measurement bicycle with rigid rider harness, parameters according to Table 4 and system matrices according to Table 5, and b): Experimental setup at UC Davis of an instrumented and actuated bicycle riding on a narrow treadmill. The lateral perturbation is an impulsive pulling force at the seat post.

Initially two different types of experiments are performed; lateral line tracking and roll stabilization of which only the latter is used here. The experiments are performed in two environments; on a horse treadmill and at the gymnasium. The horse treadmill proved to be more suitable for the perturbation experiments, since it

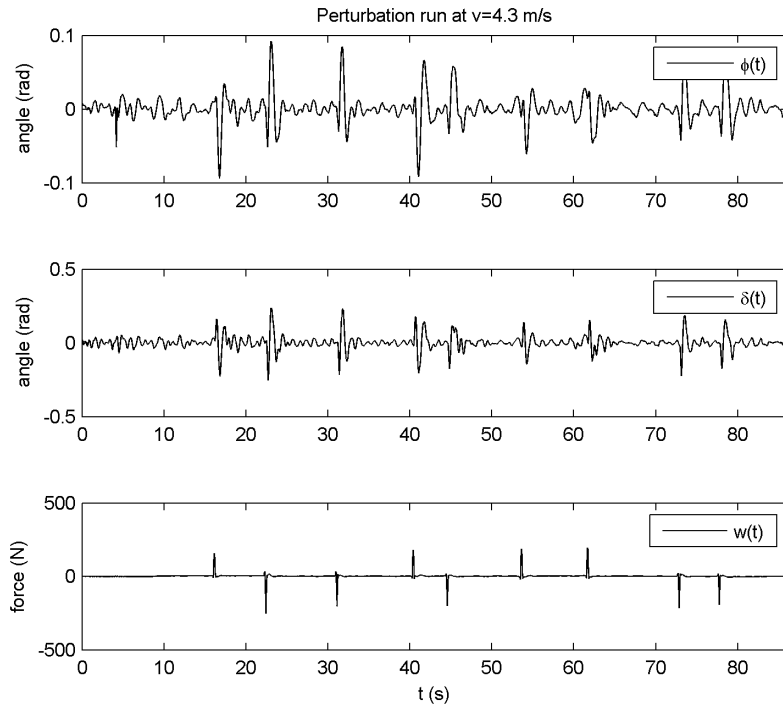


Figure 2. Measurements of the roll angle ϕ (top), steering angle δ (middle) and disturbance w (bottom) for a forward velocity of 4.3 m/s.

is more easy to perturb a stationary positioned bicycle by pulling the rope. A downside of this environment is the rather narrow track, resulting in a stressful and unnatural overly concentrated way of bicycling, which turned the roll stabilization more into heading tracking. The treadmill perturbation experiments are performed at forward velocities of about 2, 3, 4 and 7 m/s with a measurement time of $T = 60 - 90$ seconds, each of them is repeated a number of times.

The measured data during the experiment are: the forward velocity v , the rear frame roll angle ϕ and roll rate $\dot{\phi}$, the steer angle δ and steer rate $\dot{\delta}$, the disturbance force applied at the seat post w , and the steering torque T_δ . Unfortunately the measured steering torque showed a bad correlation with the one needed to drive the Whipple model in the same trajectory, it was off by a factor of 2 to 3, and was not used in the identification process. Figure 2 shows a typical measurement of the roll angle, steering angle and input force.

For further analysis, measured data from four trials are chosen, these runs are shown in Table 1. The corresponding data for these trials is publicly available and can be downloaded from [15]. These four trials are chosen, because they show a clear input/output relationship, which allows for proper system identification. Note that the first run is performed with a different rider and task description than the other three, which may make it difficult to compare with each other.

For the dynamic model of the bicycle rider combination, see Section 4, the dimensions and inertial properties of the bicycle are measured according to [17]. The resulting parameters for the rigid rider (Whipple) bicycle model are presented in Table 4, whereas in Table 5 the corresponding mass, damping and stiffness matrices together with the disturbance force transfer matrix are shown. Note that the lateral force w contributes mainly to the generalized lean torque T_ϕ and little to the generalized steer torque T_δ . This makes sense, because the rope is attached under the rider seat and is pulled in a lateral direction, which mainly causes a roll torque.

RunID	Rider	v (m/s)	T (s)	Environment	Date and Time	Task description
105	Jason	3.2	60	Horse treadmill	24-Feb-2011 18:28:23	Line tracking with disturbance
280	Luke	2.1	90	Horse treadmill	30-Aug-2011 15:38:43	Balance with Disturbance
282	Luke	4.3	90	Horse treadmill	30-Aug-2011 16:07:59	Balance with Disturbance
285	Luke	7.4	90	Horse treadmill	30-Aug-2011 16:20:52	Balance with Disturbance

Table 1. Run number used for further data analysis. Notice that the rider and task of the first entry is different from the other three.

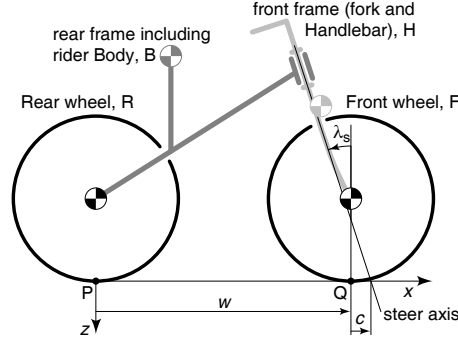


Figure 3. The bicycle model: four rigid bodies (rear wheel R, rear frame B, front handlebar assembly H, front wheel F) connected by three revolute joints (rear hub, steering axis, front hub), together with the coordinate system and the degrees of freedom.

4 SYSTEM MODEL

The total system is a combination of a bicycle and rider. For the bicycle the Whipple rigid rider model will be used. Whereas, the rider control will be modeled as a linear feedback control system with inherent neuromuscular lag and time delays.

4.1 Bicycle model

The bicycle model used is the so-called Whipple model [18], which recently has been benchmarked [1]. The model, see Figure 3, consists of four rigid bodies connected by revolute joints. The contact between the knife-edged wheels and the flat level surface is modelled by holonomic constraints in the normal direction, prescribing the wheels to touch the surface, and by non-holonomic constraints in the longitudinal and lateral directions, prescribing zero longitudinal and lateral slips. In this original model, it is assumed that the rider is rigidly attached to the rear frame and has no hands on the handlebar. The resulting non-holonomic mechanical model has three velocity degrees of freedom: forward speed v , lean rate $\dot{\phi}$ and steering rate $\dot{\delta}$.

The lateral motions can be described by the linearized equations of motion for small perturbations about the upright steady forward motion. These linearized equations of motion are fully described by Meijaard *et al.* [1]. They are expressed in terms of small changes in the lateral degrees of freedom (the rear frame roll angle, ϕ , and the steering angle, δ) from the upright straight-ahead configuration $(\phi, \delta) = (0, 0)$, at a forward speed v , and have the form

$$\mathbf{M}\ddot{\mathbf{q}} + v\mathbf{C}_1\dot{\mathbf{q}} + [g\mathbf{K}_0 + v^2\mathbf{K}_2]\mathbf{q} = \mathbf{f}, \quad (1)$$

where the time-varying variables are $\mathbf{q} = [\phi, \delta]^T$ and the lean and steering torques are $\mathbf{f} = [T_\phi, T_\delta]^T$. The coefficients in this equation are: a constant symmetric mass matrix, \mathbf{M} , a damping-like (there is no real damping) matrix, $v\mathbf{C}_1$, which is linear in the forward speed v , and a stiffness matrix which is the sum of a constant symmetric part, $g\mathbf{K}_0$, and a part, $v^2\mathbf{K}_2$, which is quadratic in the forward speed. The forces on the right-hand side, \mathbf{f} , are the applied forces which are energetically dual to the degrees of freedom \mathbf{q} . In the upright straight-ahead configuration, the linearized equation of motion for the forward motion is decoupled

from the linearized equations of motion of the lateral motions and simply reads $\dot{v} = 0$.

Besides the equations of motion, kinematic differential equations for the configuration variables that are not degrees of freedom have to be added to complete the description. For the forward motion, the equations for the rotation angles of the wheels are $\dot{\theta}_R = -v/r_R$, $\dot{\theta}_F = -v/r_F$, where θ_R and θ_F are the rotation angles of the rear and front wheel and r_R and r_F are the corresponding wheel radii. For the lateral motion, the equations for the yaw (heading) angle, ψ , and the lateral displacement of the rear and front wheel contact point, y_P and y_Q , are $\dot{\psi} = (v\delta + c\dot{\delta}) \cos \lambda_s/w$, $\dot{y}_P = v\psi$, and $y_Q = y_P + w\psi - c\delta \cos \lambda_s$, with wheelbase w , trail c , and head angle λ_s . For the case of the bicycle, these equations can be considered as a system in series with the system defined by the equations of motion (1) with \mathbf{q} and $\dot{\mathbf{q}}$ as inputs and the configuration variables as outputs.

The entries in the constant coefficient matrices \mathbf{M} , \mathbf{C}_1 , \mathbf{K}_0 and \mathbf{K}_2 can be calculated from a non-minimal set of 25 bicycle parameters as described in [1]. A procedure for measuring these parameters for a given bicycle is described in [19], whereas measured values for the bicycles used in this study are listed in Table 4 of the appendix. Then, with the coefficient matrices the characteristic equation,

$$\det(\mathbf{M}\lambda^2 + v\mathbf{C}_1\lambda + g\mathbf{K}_0 + v^2\mathbf{K}_2) = 0, \quad (2)$$

can be formed and the eigenvalues, λ , can be calculated. In principle, there are up to four eigenmodes, where oscillatory eigenmodes come in pairs. Two are significant and are traditionally called the *capsize* mode and the *weave* mode, see Figure 4. The capsize mode corresponds to a real eigenvalue with an eigenvector dominated by lean: when unstable, the bicycle follows a spiralling path with increasing curvature until it falls. The weave mode is an oscillatory motion in which the bicycle sways about the heading direction. The third remaining eigenmode is the overall stable *castering* mode, like in a trailing caster wheel, which corresponds to a large negative real eigenvalue with an eigenvector dominated by steering. The eigenvalues corresponding to the kinematic differential equations are all zero and correspond to changes in the rotation angles of the wheels, a constant yaw angle and a linearly increasing lateral displacement.

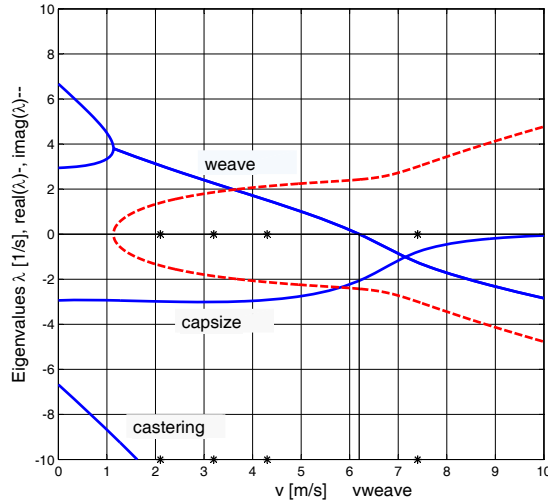


Figure 4. Eigenvalues for the uncontrolled instrumented bicycle from figure 1 in the forward speed range $0 < v < 10$ m/s, solid lines are the real values and dashed lines are the imaginary values. The speed where the weave motion becomes stable is $v_{\text{weave}} \approx 6.2$ m/s. Forward speeds used in the experiments are denoted by an *.

For control purposes it is convenient to express the bicycle equations (1) in state space form and as a set of

transfer functions. The state space representation is then give by,

$$\dot{\mathbf{x}} = \mathbf{A}\mathbf{x} + \mathbf{B}\mathbf{f} \quad (3)$$

$$\mathbf{y} = \mathbf{C}\mathbf{x} + \mathbf{D}\mathbf{f}, \quad (4)$$

whith the state vector $\mathbf{x} = [\dot{\phi}, \dot{\delta}, \phi, \delta]^T$, input vector $\mathbf{f} = [T_\phi, T_\delta]^T$, and output vector $\mathbf{y} = [\phi, \delta]^T$. The system matrix \mathbf{A} , input gain matrix \mathbf{B} , observer matrix \mathbf{C} and direct feed-through matrix \mathbf{D} are then given by,

$$\begin{aligned} \mathbf{A} &= \begin{bmatrix} -\mathbf{M}^{-1}v\mathbf{C}_1 & -\mathbf{M}^{-1}(g\mathbf{K}_0 + v^2\mathbf{K}_2) \\ \mathbf{I} & \mathbf{0} \end{bmatrix}, & \mathbf{B} &= \begin{bmatrix} \mathbf{M}^{-1} \\ \mathbf{0} \end{bmatrix}, \\ \mathbf{C} &= \begin{bmatrix} \mathbf{0} & \mathbf{I} \end{bmatrix}, & \mathbf{D} &= \begin{bmatrix} \mathbf{0} \end{bmatrix}. \end{aligned} \quad (5)$$

The state space equations can also be expressed as a set of transfer functions $\mathbf{H}_{yf}(s)$ by making use of,

$$\mathbf{y}(s) = \mathbf{H}_{yf}(s)\mathbf{f}(s), \quad \text{with} \quad \mathbf{H}_{yf}(s) = \mathbf{C}(s\mathbf{I} - \mathbf{A})^{-1}\mathbf{B} + \mathbf{D}, \quad (6)$$

where the s denotes the Laplace argument. Finally we end by introducing the reference error \mathbf{z} . Since we are interested in roll stabilization, this simply becomes $\mathbf{z} = -\phi$, resulting in the following transfer function:

$$\mathbf{z}(s) = \mathbf{H}_{zf}(s)\mathbf{f}(s), \quad \text{where} \quad \mathbf{H}_{zf}(s) = -[0, 0, 1, 0] \mathbf{H}_{yf}(s) \quad (7)$$

4.2 Rider control model

The rider control model is assumed to be a a linear feedback system in series with neuromuscular lag and time delay. The linear feedback system is usually written as

$$\mathbf{u}(s) = \mathbf{K}(s)\mathbf{y}(s), \quad (8)$$

with the control input \mathbf{y} , control output \mathbf{u} , and feedback gains $\mathbf{K}(s)$. In our model the rider control input is assumed to be the bicycle lean and steer angle, $\mathbf{y} = [\phi, \delta]^T$, and for the rider control output we assume steer torque only, $\mathbf{u} = [T_{\delta,u}]$. This rider control output then acts as input to the bicycle model, $\mathbf{f} = [0, 1]^T \mathbf{u}$, and by such closes the control loop. We assume only steer torque control because according to [16] the roll angle is mainly controlled by this, whereas the upper-body lean action is insignificant for control purpose. Moreover, during the experiments the upper-body lean is restrained by a harness connected rigidly to the bicycle. In addition the knees are also connected to the bicycle frame through a set of magnets. All together, this makes it very unlikely that the rider uses other control means than the steering control. This rider contribution to the generalized steering torque will be denoted by $T_{\delta,u}$, where the subscript u indicates the rider contribution. Next we introduce a number of sensory feedback gains, which act linearly on the bicycle configuration output. We assume the rider to be capable of sensing and applying proportional, integrative, first and second order derivative action. These assumptions may be modeled mathematically according to,

$$\begin{aligned} K_\phi(s) &= k_{\phi p} + k_{\phi i} s^{-1} + k_{\phi d} s + k_{\phi dd} s^2, \\ K_\delta(s) &= k_{\delta p} + k_{\delta i} s^{-1} + k_{\delta d} s + k_{\delta dd} s^2, \end{aligned} \quad (9)$$

with roll angle feedback K_ϕ and steer angle feedback K_δ . The gains k with subscript p, i, d and dd indicate proportional, integral, first and second order derivative gains respectively.

According to McRuer and Jex [20], the human controller is inherently limited by neuromuscular lag and time delays. Here neuromuscular dynamics of the rider arms are modeled using shoulder muscle model from [21, 22], which yields,

$$G_{nm}(s) = \frac{\omega_c^2}{s^2 + 2\zeta\omega_c + \omega_c^2}, \quad (10)$$

with cutoff frequency $\omega_c = 2.17 \cdot 2\pi$ rad/s and damping coefficient $\zeta = \sqrt{2}$. This system acts as a critically damped second order filter with a cutoff frequency equal to ω_0 . Neural transmission results in an effective time delay, which differs for visual, vestibular and muscle feedback. Such time delays have

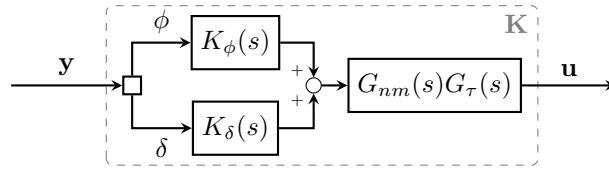


Figure 5. Block diagram of the inner control structure of \mathbf{K} , with roll and steering angle feedback gains K_ϕ and K_δ , timedelay G_τ , neuromuscular lag G_{nm} , input $\mathbf{y} = [\phi, \delta]^T$ and output $\mathbf{u} = [T_{\delta,u}]^T$.

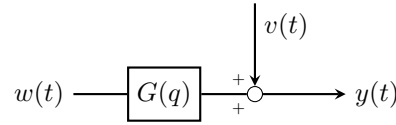


Figure 6. System description, with; output $y(t)$, input $w(t)$, disturbance $v(t)$ and system $G(q)$.

been omitted from the current study for reasons of simplicity. Sensory information regarding roll angle will derive from the visual and the vestibular system, while sensory information regarding steer angle will derive from muscle spindles in the arm. Manual control studies show that operators can apply proportional as well as lead (differential) or lag (integrator) control actions using visual task information [23]. The vestibular organ senses roll through the semicircular canals where its output is largely in phase with rotational velocity, while the otoliths sense linear acceleration, direction and magnitude of the gravitational force. The muscle spindles supply position and velocity information. The relevance and possible sensory origin of steering angle acceleration and roll acceleration will be addressed in the discussion.

Finally the human limitations and the linear feedback model are combined to form a rider control model according to,

$$\mathbf{K}(s) = G_{nm}(s)G_\tau(s) [K_\phi(s) \quad K_\delta(s)]^T, \quad (11)$$

which is presented as a block diagram in Figure 5. Note that the forward speed v serves as a parameter, such that all results depend on this since the dynamics of the bicycle is strongly forward speed dependent.

5 SYSTEM IDENTIFICATION

The rider control system identification is done in three steps. First, a nonparametric Finite Impulse Response (FIR) model is fitted to the raw data. Next, the FIR model is used to obtain a noise model. Finally, a parametric model according to (9) is used, which is optimized by using parameter reduction techniques. The analysis is performed for a number of forward speeds, resulting in a set of parametric models.

The system identification assumes a linear input/output model with additive random noise. Then the system can be described by,

$$y(t) = G(q)w(t) + v(t), \quad (12)$$

with output $y(t)$, input $w(t)$, disturbance $v(t)$ and model $G(q)$, *see* Figure 6. The q operator acts as a discrete shifting function, such that $q^{-k}w(t) = w(t - k)$. This is a convenient description, because it separates the deterministic input related contribution $G(q)w(t)$ from the stochastic contribution $v(t)$.

5.1 FIR model

The first step in the system identification is to fit a nonparametric finite impulse response (FIR) model to the measured data. After filtering, this model then can serve as a basis for the noise model. The unknown coefficient of the FIR model may be estimated by using the measured input $w(t)$ and output $y(t)$ data. The

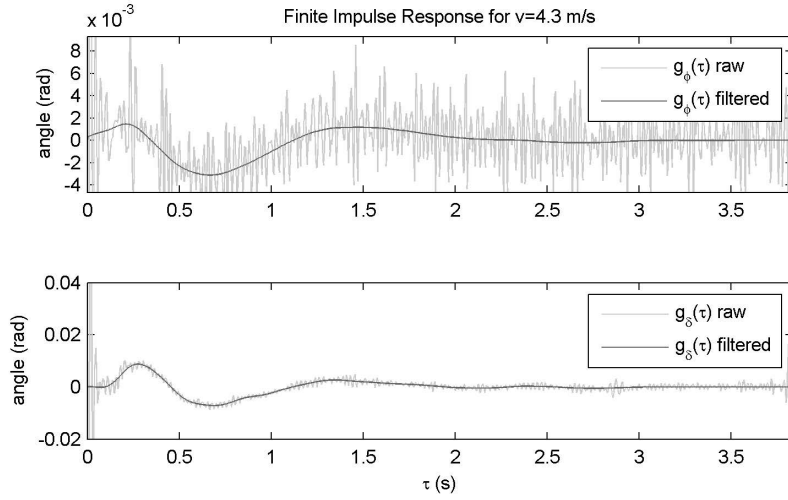


Figure 7. Finite impulse response model for the roll angle δ (top) and steering angle δ (bottom) for a forward velocity of $v = 4.3$ m/s. The raw FIR model is smoothed using a low pass filtering with a cutoff frequency of 10 Hz.

output data is either represents $y(t) = \phi$ corresponding to $G_\phi(q)$ or $y(t) = \delta(t)$ corresponding to $G_\delta(q)$. We assume a finite discrete normalized time; $t = 1, 2, 3, \dots, n$, such that the approximated output $\hat{y}(t)$ is,

$$\begin{aligned} \hat{y}(t) &= \sum_{k=1}^m \hat{g}(k) q^{-k} w(t) + v(t), \\ &= \sum_{k=1}^m \hat{g}(k) w(t-k) + v(t). \end{aligned} \quad (13)$$

From the experiment we know that no input outside the measurement interval $\{1 < t < n\}$ is applied, which can be expressed as: $w(t) = 0$ for $t < 1$ and $t > n$. The unknown coefficients $\hat{g}(k)$ can be solved from the linear quadratic optimization problem, $\hat{\mathbf{g}} = \arg \min_{\hat{\mathbf{g}}} \{(\hat{\mathbf{y}} - \mathbf{y})^2\}$. After experimenting with different finite impulse lengths, the oscillations are found to die out after $m = 768$ samples, which corresponds to finite response length of 3.84 seconds. The FIR models are smoothed by applying a low pass 8th order Butter-worth filter with a cutoff frequency of 10 Hz. The results for $v = 4.3$ m/s are shown in Figure 7.

5.2 Noise model

We can use the FIR model to estimate the disturbance $v(t)$, from (12), we obtain,

$$\hat{\mathbf{v}}(t) = \mathbf{y}(t) - \hat{\mathbf{G}}_N(q)w(t), \quad (14)$$

where $\hat{\mathbf{v}}(t) = [v_\phi(t), v_\delta(t)]^T$ is the estimated disturbance and $\hat{\mathbf{G}}_N(q) = [\hat{G}_\phi(q), \hat{G}_\delta(q)]^T$ represents the obtained non parametric impulse response model from input $w(t)$ to output $\mathbf{y}(t)$. The decomposition of the measured data into the deterministic input related component and stochastic component is shown for $v = 4.3$ m/s in Figure 8.

When analyzing the results from the FIR and the noise model, *see* Figure 7 and 8, a number of observations can be made. The high frequency noise is merely an artifact of the deconvolution proces and does not originate from the rider/bicycle system itself. The 4th and 5th peak in both the roll and steering angle response, do not seem to be very likely and may be caused by noise. The signal to noise ratio for the case $v = 2.1$ m/s (not shown here) is very low, resulting in an unreliable FIR model. The signal to noise ratio of the steering angle response is generally of better quality than the roll angle response. The overall shape of the roll and steering angle responses are similar, but the amplitudes and time characteristics differ.

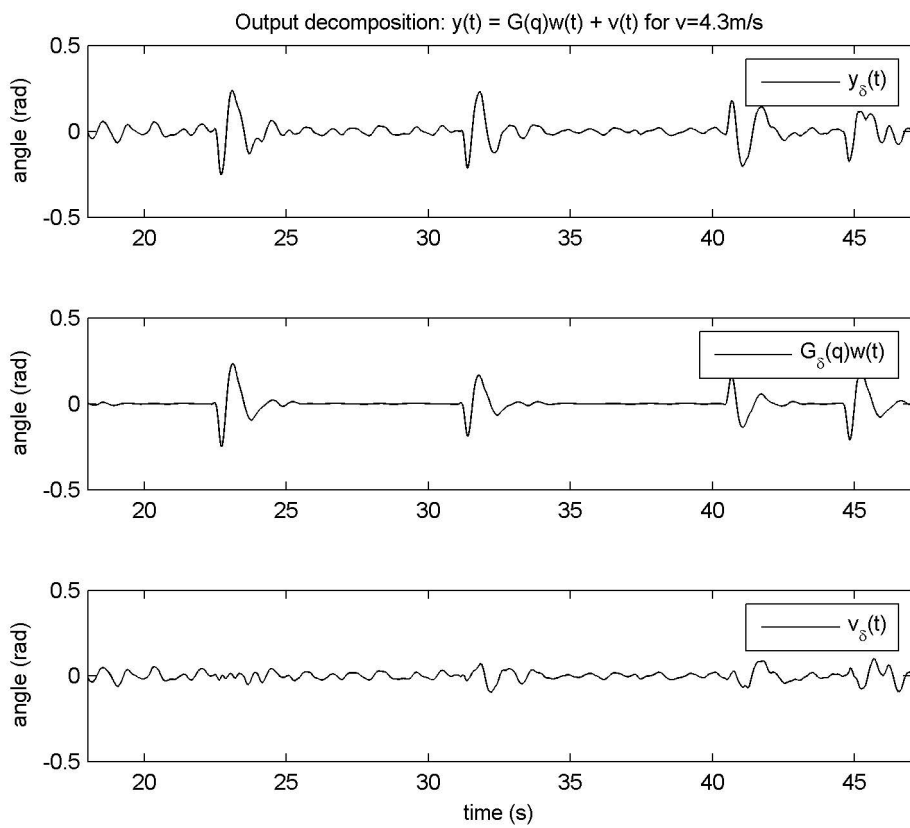


Figure 8. Output decomposition of the steering angle output $y(t)$ in terms of input related component $G(q)w(t)$ and remnant component $v(t)$ for a forward velocity of $v = 4.3$ m/s.

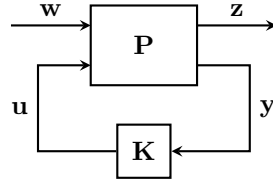


Figure 9. Block diagram of the general control description, with known bicycle dynamics \mathbf{P} , unknown controller \mathbf{K} , disturbance input \mathbf{w} , error output $\mathbf{z} = -\phi$, control input \mathbf{y} and control output \mathbf{u} .

The amplitude of the oscillation decreases as the forward velocity increases. The impulse response seems to damp out more quickly as the forward velocity increases, which we would expect from the eigenvalue analysis on the uncontrolled bicycle model.

5.3 Parametric model

In the parametric rider control model the parameters are the unknown gains from (9). The complete system model, the bicycle model together with the feedback control model, is shown in Figure 9. The corresponding parametric model structure is then given by,

$$\mathbf{y}(\boldsymbol{\theta}) = \mathbf{G}(\boldsymbol{\theta})\mathbf{w}, \quad \mathbf{G}(\boldsymbol{\theta}) = \left[\mathbf{P}_{yw} + \mathbf{P}_{yu}(\mathbf{I} - \mathbf{K}(\boldsymbol{\theta})\mathbf{P}_{yu})^{-1} \mathbf{K}(\boldsymbol{\theta})\mathbf{P}_{yw} \right], \quad (15)$$

with bicycle dynamics \mathbf{P}_{yw} and \mathbf{P}_{yu} , human controller $\mathbf{K}(\boldsymbol{\theta})$ with the unknown gains k defined as the model parameters $\boldsymbol{\theta}$, disturbance input $\mathbf{w} = w$ and output $\mathbf{y} = [\phi, \delta]^T$. Notice that only the human controller model is unknown, while the bicycle dynamics are known since they are determined a priori from the bicycle model (5).

The error criterium used to estimate the parameters $\boldsymbol{\theta}$ is based on a weighted quadratic sum,

$$V_N(\boldsymbol{\theta}) = \frac{1}{N} \sum_{t=1}^N \left[\left(\hat{G}_\delta(q) - G_\delta(q, \boldsymbol{\theta}) \right) w(t) \right]^2, \quad (16)$$

where the difference between the nonparametric (FIR) and parametric models is weighted by the input signal w . Here we only use the steering angle response because the rider directly excites the steering dynamics and it is expected that the steering signal contains the most direct information concerning rider actions. The initial parameter vector $\boldsymbol{\theta}_0$ is determined by a random search method, for which the lowest criterium score is further optimized by using the `lsqnonlin` function. The parameter optimization results in a optimal parameter vector set according to,

$$\hat{\boldsymbol{\theta}} = \arg \min_{\boldsymbol{\theta}} V_N(\boldsymbol{\theta}), \quad (17)$$

The parametric modeling is performed for several cases, where the forward velocity takes the following values: 2.1, 3.2, 4.3 and 7.4 m/s. Numerical issues were encountered with the rider model with time delays. For the current study the problem is circumvented by ignoring the time delay by setting it to zero.

The results from the parametric model for a forward velocity of $v = 4.3$ m/s are shown in Figure 10. The comparison of this parameter model response to the FIR model are shown in Figure 11.

Finally, we apply a parameter reduction technique to determine the essential feedback loops in the rider control system. The reduction is based on the quality of the fit and selection of parameters guided by the parameter covariance as defined by Ljung [24]. The quality of the fit is measured by the Variance Accounted For (VAF), which is defined as the normalized difference between modeled output and measured output,

$$\text{VAF}(\boldsymbol{\theta}) = 1 - \frac{\sum_{t=1}^n (e(t, \boldsymbol{\theta})^2)}{\sum_{t=1}^n (y(t)^2)}, \quad \text{with} \quad e(t, \boldsymbol{\theta}) = y(t) - \hat{y}(t, \boldsymbol{\theta}). \quad (18)$$

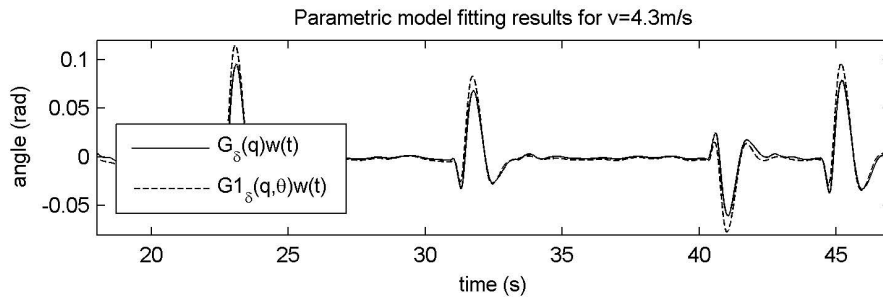


Figure 10. Comparison of the noise filtered FIR, G_δ , and the parameter fitted model response $G1_\delta$ of the steer angle δ , at a forward speed of $v = 4.3$ m/s.

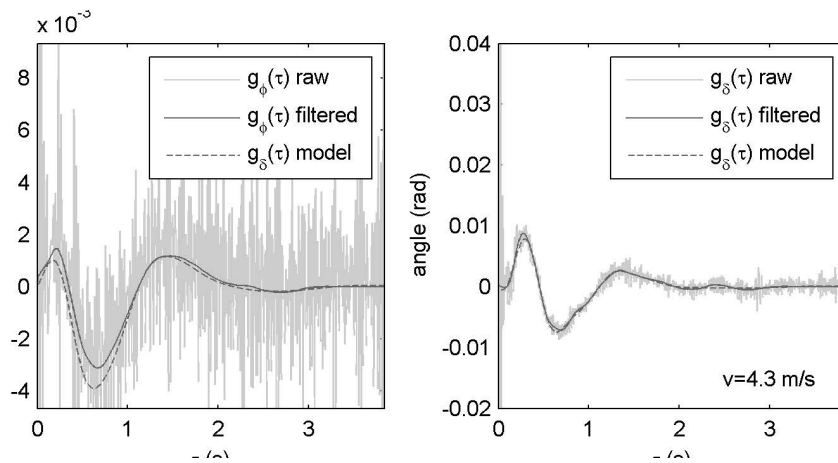


Figure 11. Zoomed in comparison of the raw FIR, the noise filtered FIR and the parameter fitted model response of lean angle ϕ (left) and the steer angle δ (right), at a forward speed of $v = 4.3$ m/s.

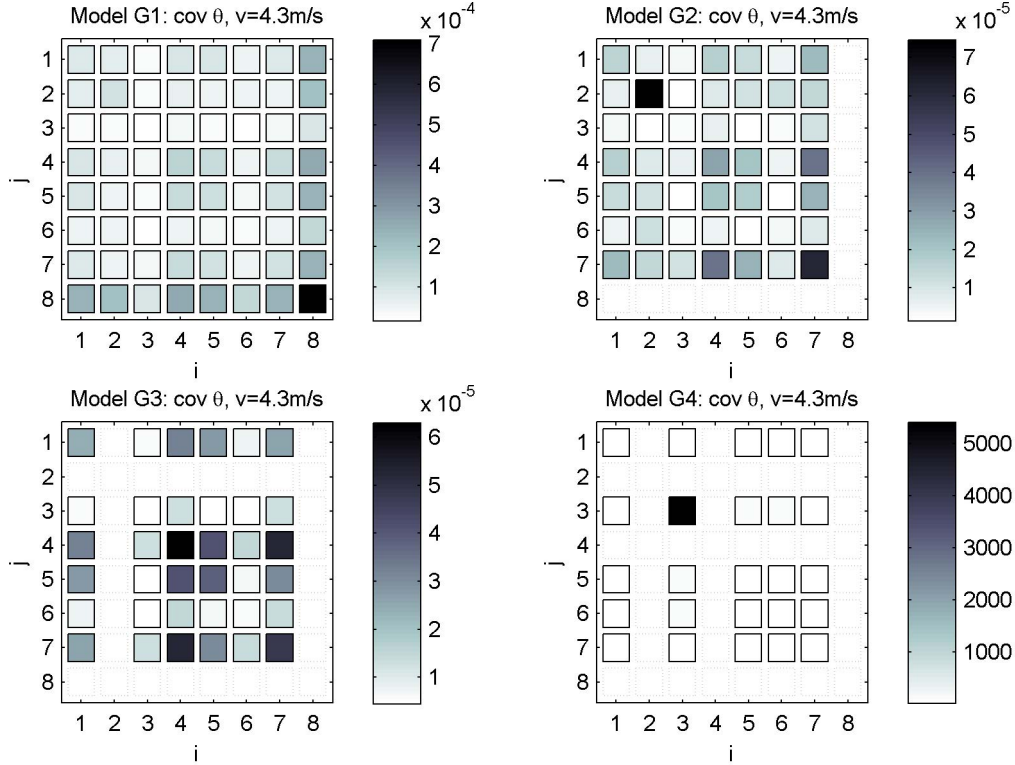


Figure 12. Subsequent parameter covariance matrices after iterative parameter reduction. The parametric model for a forward velocity of $v = 4.3$ m/s. The parameter space is reduced by one for each iteration until the VAF value drops down dramatically. The subsequent VAF values are: (99.31, 99.26, 98.75, 0.00)%.

where a VAF score of 1 means a perfect fit. The sensitivity of the quality of the fit with respect to the parameters θ is defined by the parameter covariance,

$$\text{cov } \theta_{ij} = \rho \left[\frac{1}{n} \sum_{t=1}^n \psi(t, \theta_i) \psi(t, \theta_j) \right]^{-1}, \quad \text{with} \quad \rho = \frac{1}{n} \sum_{t=1}^n [e(t, \theta)]^2, \quad (19)$$

and with the partial derivative of the error $e(t, \theta)$ with respect to the i^{th} parameters θ_i defined as

$$\psi(t, \theta_i) = -\frac{d}{d\theta_i} e(t, \theta) = \frac{d}{d\theta_i} \hat{y}(t, \theta) \quad (20)$$

Instead of calculating all $8! = 40320$ possible combinations, we start from a full parameter set and guided by the parameter covariance select the parameter which has the least influence on the quality of the fit. This process is repeated until the quality of the fit drops below a certain threshold, f.i. 50%. An example of this parameter reduction process, for $v = 4.3$ m/s, is shown in Figure 12, whereas the results for all three forward speeds is presented in Table 2. These results will be discussed in the next section.

Finally we check the stability of the system by calculating the eigenvalues for the the closed loop system with the set of reduced control model parameters, *see* Table 3. We observe that the state has increased from 4 to 7 dimensions. Two states are added due to the neuromuscular activation dynamics G_{nm} , which acts as a second order low pass filter on the controller output and one state is added due to the integrative feedback action on the steering angle. The real parts of all eigenvalues are negative, which indicates stability. If we compare these results to the open loop uncontrolled dynamics, as represented by the eigenvalues from Figure 4, we see that unstable roots at forward speeds $v = 3.2$ and $v = 4.3$ m/s are clearly stabilized.

Model	$k_{\phi p}$	$k_{\phi i}$	$k_{\phi d}$	$k_{\phi dd}$	$k_{\delta p}$	$k_{\delta i}$	$k_{\delta d}$	$k_{\delta dd}$	VAF
$\mathbf{K}(s, \boldsymbol{\theta}(v = 3.2))$	81.41	-7.68	57.99	-1.98	-8.10	182.73	-6.98	-0.21	97.56
	79.48		57.50	-2.00	-8.19	177.40	-6.99	-0.20	97.56
	54.66		50.20	-0.87		147.99	-5.30	-0.13	97.33
	52.18		43.51			131.94	-3.97	-0.14	97.09
	36.81		32.99			89.45	-3.25		94.24
			32.80			90.91	-1.72		0.00
$\mathbf{K}(s, \boldsymbol{\theta}(v = 4.3))$	44.93	-56.22	39.65	1.16	16.25	277.79	-3.10	-0.05	99.31
	29.98	-40.27	33.78	1.60	21.72	222.31	-2.05		99.26
	29.58		33.79	1.26	17.08	195.40	-2.74		98.75
	299.44		0.87		-54.16	-446.57	-16.06		0.00
$\mathbf{K}(s, \boldsymbol{\theta}(v = 7.4))$	97.95	-128.03	58.78	-0.63	-30.42	1424.31	-14.10	-0.19	96.15
	77.81	-108.86	51.84		-1.34	1230.16	-11.43	-0.13	96.12
	76.54	-108.23	51.83			1226.80	-11.44	-0.12	96.11
	62.40	-42.25	42.19			886.86	-10.34		95.25
	59.20		41.56			816.11	-10.56		95.06
			68.98			1372.49	-19.47		0.00

Table 2. Overview of parametric modeling results, with controller \mathbf{K} , parameter vector $\boldsymbol{\theta}$, forward velocity v (m/s), roll proportional gain $k_{\phi p}$ (Nm/rad), roll integrative gain $k_{\phi i}$ (Nm/s rad), roll derivative gain $k_{\phi d}$ (Nm s/rad), roll 2nd derivative gain $k_{\phi dd}$ (Nm s²/rad), steer proportional gain $k_{\delta p}$ (Nm/rad), steer integrative gain $k_{\delta i}$ (Nm/s rad), steer derivative gain $k_{\delta d}$ (Nm s/rad), steer 2nd derivative gain $k_{\delta dd}$ (Nm s²/rad) and Variance Accounted For VAF (%). The grey marked rows indicate the reduced parametric models which have a minimal number of parameters and still show a good fit (VAF > 95%).

	$\mathbf{K}(s, \boldsymbol{\theta}(v = 3.2))$	$\mathbf{K}(s, \boldsymbol{\theta}(v = 4.3))$	$\mathbf{K}(s, \boldsymbol{\theta}(v = 7.4))$
λ	-22.76	-25.08	-36.57
	-1.70 ±11.53 <i>i</i>	-2.31 ±13.12 <i>i</i>	-2.18 ±17.86 <i>i</i>
	-1.40 ±5.25 <i>i</i>	-1.88 ±5.76 <i>i</i>	-1.93 ±7.26 <i>i</i>
	-1.16 ±2.60 <i>i</i>	-0.99 ±2.99 <i>i</i>	-1.27 ±2.91 <i>i</i>

Table 3. Closed loop eigenvalues $\lambda = \text{eig}(\mathbf{G}(s, \boldsymbol{\theta}))$ for the selected reduced parametric models from Table 2.

6 DISCUSSION

The values for the linear feedback rider control model according to Figure 5 and equation (9), for all three forward speeds, are presented in Table 2, from which the the following observations can be made. The resulting identified parametric model with eight feedback gains accounts for 97% of the variance of the non parametric model output. However, the parameters set can be reduced to only four gains while retaining 94% of the variance: a gain on the lean angle and lean rate and a gain on the steer rate and the integral of the steer angle. The use of lean angle and rate represents vestibular and/or visual feedback, and the use of steer angle rate represents proprioceptive feedback. The sign of the gains on the lean angle and lean rate clearly show that the steer-into-the-fall balance principle [2] is used by the rider. The feedback of the integral of the steer angle can be explained by the need for the rider to stay on the the narrow treadmill. Here the rider is controlling the heading of the bicycle within small bounds and the heading is mainly determined by the integral of the steer angle. All feedback gains show a forward speed dependency, the most profound in the integral steering feedback, which seems to be quadratic in the forward speed.

7 CONCLUSIONS

Rider control in bicycling is identified by a linear feedback control model where muscle dynamics are incorporated. The measured data was obtained while riding on a narrow treadmill where the system was perturbed by an intermittent lateral impulsive force. The identified rider control model with the reduced parameter set stabilizes the system, follows the necessary stability condition of steer into the fall and seems to mimic human control in a natural way. Future research will be conducted to obtain experiment data of bicycling on the open road, where the restricting of keeping a narrow lane, like on the treadmill, is released. The same techniques as described in this paper can then be used to obtain a pure stabilizing rider control model.

REFERENCES

- [1] J. P. Meijaard, Jim M. Papadopoulos, Andy Ruina, and A. L. Schwab. Linearized dynamics equations for the balance and steer of a bicycle: a benchmark and review. *Proceedings of the Royal Society A*, 463:1955–1982, 2007.
- [2] J. D. G. Kooijman, J. P. Meijaard, Jim P. Papadopoulos, Andy Ruina, and A. L. Schwab. A bicycle can be self-stable without gyroscopic or caster effects. *Science*, 332:339–342, April 15, 2011.
- [3] A. van Lunteren and H. G. Stassen. On the variance of the bicycle rider’s behavior. In *Proceedings of the 6th Annual Conference on Manual Control*, April 1970.
- [4] Roy S. Rice and R. Douglas Roland. An evaluation of the performance and handling qualities of bicycles. Technical report, Cornell Aero. Lab. Rept. VJ-2888-K, April 1970. (available at: <http://bicycle.tudelft.nl/schwab/Bicycle/calspan/>).
- [5] D. H. Weir. *Motorcycle Handling Dynamics and Rider Control and the Effect of Design Configuration on Response and Performance*. PhD thesis, University of California, LA, 1972.
- [6] D.J. Eaton. *Man-Machine Dynamics in the Stabilization of Single-Track Vehicles*. PhD thesis, University of Michigan, 1973.
- [7] R. S. Sharp. The stability and control of motorcycles. *Journal of Mechanical Engineering Science*, 13(5):316–329, 1971.
- [8] A. A. Popov, S. Rowell, and J. P. Meijaard. A review on motorcycle and rider modelling for steering control. *Vehicle System Dynamics*, 48:775–792, 2010.
- [9] Jason K. Moore, J. D. G. Kooijman, A. L. Schwab, and Mont Hubbard. Rider motion identification during normal bicycling by means of principal component analysis. *Multibody System Dynamics*, 25(2):225–244, 2011.

- [10] Duane T. McRuer, Dunstan Graham, and Ezra S. Krendel. Manual control of single-loop systems: Part i. *Journal of the Franklin Institute*, 283(1):1 – 29, 1967.
- [11] Duane T. McRuer, Dunstan Graham, and Ezra S. Krendel. Manual control of single-loop systems: Part ii. *Journal of the Franklin Institute*, 283(2):145 – 168, 1967.
- [12] D.T. McRuer, R.W. Allen, D.H. Weir, and R.H. Klein. New results in driver steering control models. *Human Factors: The Journal of the Human Factors and Ergonomics Society*, 19(4):381–397, 1977.
- [13] A. J. R. Doyle. *The skill of bicycle riding*. PhD thesis, University of Sheffield, UK, 1987. (available at: <http://bicycle.tudelft.nl/schwab/Bicycle/doyle1987skill.pdf>).
- [14] J. Milton, J.L. Cabrera, T. Ohira, S. Tajima, Y. Tonosaki, C.W. Eurich, and S.A. Campbell. The time-delayed inverted pendulum: Implications for human balance control. *Chaos: An Interdisciplinary Journal of Nonlinear Science*, 19:026110, 2009.
- [15] <http://biosport.ucdavis.edu/research-projects/bicycle/instrumented-bicycle>.
- [16] J. D. G. Kooijman, A. L. Schwab, and J. K. Moore. Some observations on human control of a bicycle. In *Proceedings of the ASME 2009 International Design Engineering Technical Conferences & Computers and Information in Engineering Conference*, DETC2009, Aug 30 – Sep 2, 2009, San Diego, CA, 2009.
- [17] J. K. Moore, M. Hubbard, J. D. G. Kooijman, and A. L. Schwab. A method for estimating physical properties of a combined bicycle and rider. In *Proceedings of the ASME 2009 International Design Engineering Technical Conferences & Computers and Information in Engineering Conference*, DETC2009, Aug 30 – Sep 2, 2009, San Diego, CA, 2009.
- [18] F. J. W. Whipple. The stability of the motion of a bicycle. *Quarterly Journal of Pure and Applied Mathematics*, 30:312–348, 1899.
- [19] J. D. G. Kooijman, A. L. Schwab, and J. P. Meijaard. Experimental validation of a model of an uncontrolled bicycle. *Multibody System Dynamics*, 19:115–132, 2008.
- [20] D.T. McRuer and H.R. Jex. A review of quasi-linear pilot models. *Human Factors in Electronics, IEEE Transactions on*, HFE-8(3):231–249, Sept. 1967.
- [21] E. de Vlugt, A.C. Schouten, and F.C.T. van der Helm. Closed-loop multivariable system identification for the characterization of the dynamic arm compliance using continuous force disturbances: a model study. *Journal of neuroscience methods*, 122(2):123–140, 2003.
- [22] R. Happee, E. De Vlugt, and A.C. Schouten. Posture maintenance of the human upper extremity; identification of intrinsic and reflex based contributions. *SAE International Journal of Passenger Cars-Mechanical Systems*, 1(1):1125, 2009.
- [23] D. T. McRuer and E. S. Krendel. Dynamic response of human operators. Technical Report WADC-TR-56-524, Wright Air Development Center, Oct. 1957.
- [24] L. Ljung. *System identification: theory for the user*, volume 11. Prentice-Hall Englewood Cliffs, NJ, 1987.

Appendices

A Bicycle parameters

Parameter	Symbol	Values
Wheel base	w	1.0759 m
Trail	c	0.0718 m
Steer axis tilt	λ_s	20.1°
Gravity	g	9.81 N/kg
Forward speed	v	various m/s
Rear wheel R		
Radius	r_R	0.3325 m
Mass	m_R	4.90 kg
Inertia	(I_{Rxx}, I_{Ryy})	(0.0701, 0.12934) kgm ²
Rear Body and frame assembly B		
Centre of mass	(x_B, z_B)	(0.33235, -1.02217) m
Mass	m_B	106.40 kg
Inertia	$\begin{bmatrix} I_{Bxx} & 0 & I_{Bxz} \\ 0 & I_{Byy} & 0 \\ I_{Bxz} & 0 & I_{Bzz} \end{bmatrix}$	$\begin{bmatrix} 13.9967 & 0 & -0.6113 \\ 0 & 15.4633 & 0 \\ -0.6113 & 0 & 4.4282 \end{bmatrix}$ kgm ²
Front Handlebar and fork assembly H		
Centre of mass	(x_H, z_H)	(0.8092, -0.9774) m
Mass	m_H	5.40 kg
Inertia	$\begin{bmatrix} I_{Hxx} & 0 & I_{Hxz} \\ 0 & I_{Hyy} & 0 \\ I_{Hxz} & 0 & I_{Hzz} \end{bmatrix}$	$\begin{bmatrix} 0.3376 & 0 & -0.0996 \\ 0 & 0.3399 & 0 \\ -0.0996 & 0 & 0.1094 \end{bmatrix}$ kgm ²
Front wheel F		
Radius	r_F	0.3356 m
Mass	m_F	1.55 kg
Inertia	(I_{Fxx}, I_{Fyy})	(0.0524, 0.0984) kgm ²

Table 4. Parameters for the measurement bicycle plus rigid rider from Figure 1 for the bicycle model from Figure 3.

$$\mathbf{M}_0 = \begin{bmatrix} 131.5085 & 2.6812 \\ 2.6812 & 0.2495 \end{bmatrix}, \mathbf{C}_1 = \begin{bmatrix} 0 & 42.748 \\ -0.31806 & 1.6022 \end{bmatrix}, \mathbf{K}_0 = \begin{bmatrix} -116.19 & -2.7633 \\ -2.7633 & -0.94874 \end{bmatrix}, \mathbf{K}_2 = \begin{bmatrix} 0 & 102.02 \\ 0 & 2.5001 \end{bmatrix},$$

$$\mathbf{H}_{fw} = \begin{bmatrix} 0.91 \\ 0.014408 \end{bmatrix}.$$

Table 5. Mass, damping and stiffness matrices (1) for the bicycle model from Figure 3 and 1 according to the parameters from Table 4, together with the transfer matrix \mathbf{H}_{fw} which maps the lateral force applied at the seat post to the generalized forces from the bicycle model.